

End-to-End Deep Learning for Reliable Cardiac Activity Monitoring using Seismocardiograms

Prithvi Suresh^α, Naveen Narayanan^β, Chakilam Vijay Pranav^γ, Vineeth Vijayaraghavan^ε

^{αγ}εSolarillion Foundation, Chennai, India

^βSSN College of Engineering, Chennai, India

{prithvisuresh^α, vineethv^ε}@ieee.org

naveen17097@cse.ssn.edu.in^β

cvpranav@gmail.com^γ

Abstract—Continuous monitoring of cardiac activity is paramount to understanding the functioning of the heart in addition to identifying precursors to conditions such as Atrial Fibrillation. Through continuous cardiac monitoring, early indications of any potential disorder can be detected before the actual event, allowing timely preventive measures to be taken. Electrocardiography (ECG) is an established standard for monitoring the function of the heart for clinical and non-clinical applications, but its electrode-based implementation makes it cumbersome, especially for uninterrupted monitoring. Hence we propose SeismoNet, a Deep Convolutional Neural Network which aims to provide an end-to-end solution to robustly observe heart activity from Seismocardiogram (SCG) signals. These SCG signals are motion-based and can be acquired in an easy, user-friendly fashion. Furthermore, the use of deep learning enables the detection of R-peaks directly from SCG signals in spite of their noise-ridden morphology and obviates the need for extracting hand-crafted features. SeismoNet was modelled on the publicly available CEBS dataset and achieved a high overall Sensitivity and Positive Predictive Value of 0.98 and 0.98 respectively.

Index Terms—Seismocardiography, Deep Learning, sig2sig, Electrocardiography, cardiac monitoring, ML for Health

I. INTRODUCTION

In the last decade, the requirement for continuous, non-intrusive monitoring of cardiac activity has significantly increased. From athletes donning a network of sensors to maximize their performance to people at risk of post-operative complications, there is a dire need for continuous surveillance of the activity of the heart. Studies on cardiac disorders such as Atrial Fibrillation [1] and Essential Hypertension [2] show that a thorough analysis of the history of the patient’s physiological signals can help avoid such catastrophes. This furthers the need for discreet cardiac monitoring.

The Electrocardiogram (ECG) has served as the gold standard measurement of information pertaining to the function of the heart for more than a century [3]. This information is obtained from the acquired ECG by detecting and processing R-peaks using various methods [4], [5] and extracting additional information such as Heart Rate Variability (HRV) indices. Despite the ECG providing accurate measurements of the cardiac activity, it suffers from a number of limitations. This renders it incapable of adapting to the surge in requirement of non-intrusive monitoring. ECG acquisition systems require

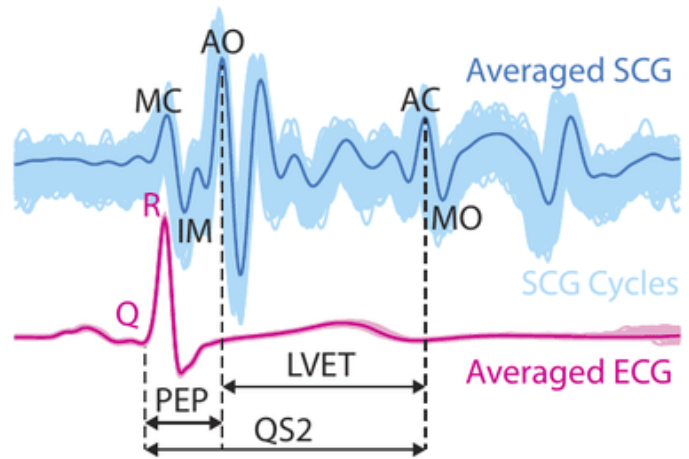


Fig. 1. SCG signal vs ECG signal Adapted from [7]

proper placement of electrodes to avoid motion artifacts. This requires a healthcare professional, who might not be available on call in developing countries and rural areas. Additionally, noise free ECG signals require direct and clean skin contact which calls for obtrusive electrode placement. This makes the process of ECG acquisition stressful to patients at the best, or prone to infection or irritation of the skin at the worst [6].

Another physiological signal used in cardiac monitoring is the Seismocardiogram (SCG). Seismocardiography is the monitoring of cardiac activity by measuring the acceleration produced at the sternum due to mechanical vibrations generated by myocardial motion [8], [9]. Since SCG signals are extracted from the surface of the chest wall, its acquisition is less obtrusive than that of the ECG. Additionally, they can be implemented via inexpensive, miniaturized micro-electro-mechanical sensors [10] that do not require an adhesive or conducting gel to be placed on the body. A combination of these factors allows for SCG to be non-intrusive, safe and viable for continuous surveillance. However, the morphology of the SCG signal is not similar to the ECG signal, as seen in Fig. 1. Though the SCG is capable of yielding similar HRV indices as compared to those extracted from the ECG, it is still prone to errors since the SCG is extremely susceptible to motion artifacts [11].

Acknowledging the advantages and shortcomings of both these signals, we propose to derive utility from SCG signals by monitoring cardiac activity and extracting information regarding the same. In this work, we introduce a Deep Fully Convolutional Neural Network which overcomes the lack of information in the SCG pertaining to the R-peak and robustly learns inherent patterns denoting the R-peaks' accurate position. This allows for non-invasive and safe monitoring of cardiac activity through an inexpensive, widely available sensor. The HRV indices obtained from the results of the model showcase the potential of the SCG to be used in reliable HRV monitoring.

II. RELATED WORK

Over the past few decades, extensive research examining the viability of utilizing SCG signals to extract cardiac activity has been undertaken. Tadi *et al.* [9] warrants the use of SCG to obtain HRV indices by detecting the interval between consecutive Arterial Openings (AO). However, this approach required fiducial points of the ECG. In the following year, Tadi *et al.* goes on to propose real-time cardiac monitoring by applying Hilbert Transform on SCG signals [12]. This approach did not require the ECG and demonstrated the viability of the SCG as a standalone signal for cardiac monitoring. Both these works prove that the HRV parameters derived from the SCG show a high correlation with the parameters extracted from ECG signals as verified by Siecinski *et al.* [13]. In these works, a signal processing approach is taken, where complex and computationally intensive algorithms which comprise of a cascade of signal processing operations such as filtering, noise-removal, segmentation and feature extraction for peak finding are employed.

Using SCG to monitor cardiac activity with smart devices in a real-time setting has been explored by the likes of Haesher *et al.* [14], [15] and Hernandez *et al.* [16], [17]. Similar to prior work, these make use of a barrage of signal processing algorithms and transforms. Additionally, AO peaks, which temporally occur after the R-peak in an ECG signal (refer Fig. 1), are used as the fiducial points to measure heart activity with the underlying assumption that the AO-AO intervals in an SCG signal correspond to the R-R intervals in an ECG signal. This is however not the case in a real-time setting where the morphology of an SCG signal is affected by many factors other than cardiac activity [18] which renders them prone to noise as shown in Fig. 2a. This consequentially makes it much more challenging to perform peak detection on them.

Recently, there has been acknowledgement of the virtues of application of Machine Learning (ML) and Deep Learning (DL) to analyze SCG signals and derive descriptive and predictive information from them. Yao *et al.* [19] presents a three layer artificial neural network that uses a combination of both ECG and SCG signals on a beat-by-beat basis for personalized quiescence prediction. Though this is applied specifically to the field of Coronary Computed Tomography Angiography, it portrays the successful application of ML to SCG signals. Mora *et al.* [20] explored the application of unsupervised

learning on SCG signals through the use of a variational autoencoder which was used to extract user information from their corresponding SCG waveforms. Haescher *et al.* [21] proposed a strategy which aims to transform SCG signals into ECG signals using a convolutional autoencoder. This was followed by the use of the Pan Tompkins algorithm [22] for R-peak detection on the resultant of the transformation. The algorithm has been studied on noise ridden ECG which showed deteriorating performance [23].

Despite a continuously rising number of devices monitoring non-medical grade signals in everyday life, there is still a dearth of reliable analysis of these signals. By leveraging end-to-end deep learning, the gap between non-clinical signal acquisition and reliable signal analysis can be bridged. We attempt to bridge this gap by proposing an end-to-end deep learning network that robustly extracts information from the prevalent SCG signals.

III. PROBLEM STATEMENT

Although existing solutions to non-invasive cardiac monitoring through SCG signals are competent, there is still a lack of an end-to-end solution which is computationally inexpensive. Existing solutions do not take into account the morphological changes that the SCG might undergo in a real-time setting. Additionally, standalone SCG signal monitoring loses out on vital information regarding the R-peaks, thus generating inaccurate HRV indices.

Considering the aforementioned drawbacks that current solutions possess, we propose *SeismoNet*, a Deep Fully Convolutional Neural Network. *SeismoNet* accurately detects R-peaks and hence provides robust monitoring of the SCG signal. This is achieved by training *SeismoNet* in an end-to-end manner to detect position of the R-peaks in spite of noise. This also dismisses the need for multiple signal processing blocks that are computationally taxing. The ease of signal acquisition of the SCG coupled with the reliability of *SeismoNet* facilitates user-friendly, non-invasive and continuous heart monitoring.

IV. METHODOLOGY

A. Dataset Description and Preprocessing

The experiments were carried out on the Combined Measurement of ECG, Breathing and Seismocardiograms (CEBS) dataset, publicly available as part of Physiobank [24]. The dataset consists of SCG, Respiratory and ECG signals from 2 leads (leads I and II), sampled at 5kHz. The data was collected from 20 subjects with no known ailments with a mean age of 24.4 years (SD \pm 3.10). The signals were acquired via a Biopac MP36. Out of the 20 subjects only 18 were considered since subject 4 and subject 18 had discrepancies during data collection.

The protocol for data collection required subjects to lie in a supine position. Recordings were first obtained from the subject while they were in the basal state. Following this, subjects were made to listen to music while the collection procedure continued. The procedure was terminated 5 minutes after the music session ended.

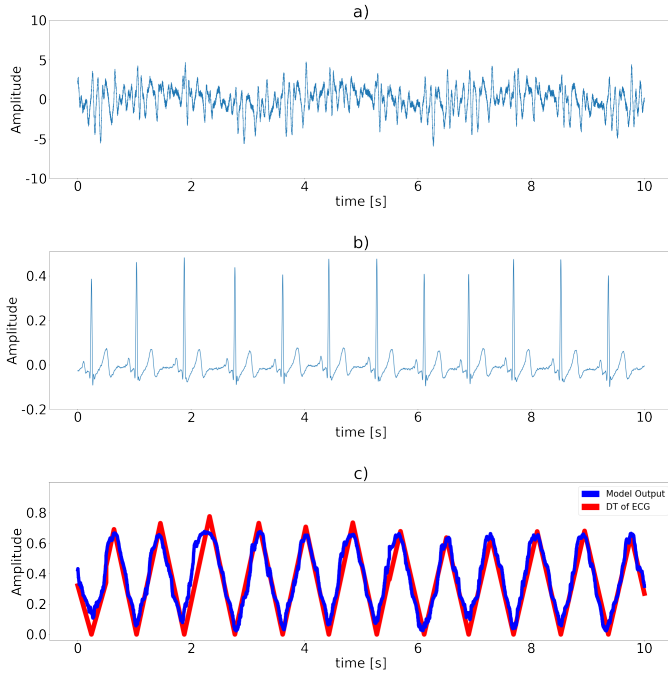


Fig. 2. a) SCG signal b) Corresponding ECG signal used for deriving ground truth c) Model Output vs Distance transform (DT) of ECG

The lead I ECG (e) and SCG (s) from each subject’s data were segmented into windows of length (w) 10 seconds with 5 seconds overlap. No filtering was performed on the SCG to best replicate real-time data reception. The resultant windows from each subject were split into 3 sections (60%-20%-20%) for training (X), validation (V) and testing (T) respectively.

B. Signal Paradigm

We propose an architecture that transforms the SCG signal ($s^{(i)}$, $s^{(i)} \in X$) into an interpretable waveform consisting of relevant information pertaining to the corresponding ECG signal ($e^{(i)}$). This allows for extraction of heart rate indices through elementary algorithms that have almost no latency. Thus, a signal-to-signal model is used whose architecture is elaborated in the following section.

SeismoNet maps the SCG signal to a transformed ECG signal ($t_{gt}^{(i)}$), wherein $t_{gt}^{(i)} = DT(e^{(i)})$ is the Distance Transform of the ECG signal. Traditionally used in Computer Vision applications [25], [26], Distance Transforms are used to map the distance of a pixel to another pixel of a specific type (such as a boundary pixel). Accordingly, the Distance Transform of an ECG signal is defined as the distance between each sample in the signal to the closest R-peak annotation. This results in a transformed signal as shown in Fig. 2c. The valleys of this transformed signal signify the position of the R-peak.

Thus, it is necessary to optimize the weights of the model to produce a signal that resembles $t_{gt}^{(i)}$. This is carried out by minimizing the $Smooth_{L1}$ loss between the prediction of the model ($t_{pred}^{(i)}$) and the ground truth ($t_{gt}^{(i)}$). The loss function \mathcal{L}

is given by

$$\mathcal{L} = \sum_{i=1}^m Smooth_{L1}(t_{pred}^{(i)} - t_{gt}^{(i)}) \quad (1)$$

$$Smooth_{L1}(x) = \begin{cases} 0.5x^2, & \text{if } |x| < 1 \\ |x| - 0.5, & \text{otherwise} \end{cases} \quad (2)$$

C. SeismoNet Architecture

The architecture of SeismoNet is an extension of the U-net framework proposed by Ronneberger *et al.* [27]. The U-net repeatedly contracts (contracting path) the input, followed by repeated expansion (expanding path) until the same dimensions of the input is obtained, akin to a standard encoder-decoder. U-net uses skip connections that connect the activations learnt by the deeper layers to the shallower layers.

The architecture proposed is broken down into blocks depending on their purpose. There are a total of $2N + 2$ blocks in the network made up of N Contracting Convolutional Blocks (CCB), N Expanding Convolutional Blocks (ECB), 1 Convolutional Ensemble Averaging Block and 1 Denoising Block. The Inception-Residual Block has been excluded while counting since it features repeatedly in other blocks. The purpose and structure of each block is as follows:

- 1) **Inception-Residual Block:** The Inception-Residual block consists of multiple convolutions¹ with different kernel sizes performed in parallel as shown in Fig. 4. Following this, channel wise concatenation of these representations is done. Furthermore, a residual connection is introduced to alleviate vanishing gradients.
- 2) **Contracting Convolutional Block (CCB):** Each Contracting Convolutional Block (C_n^c , where $n \in [1, N]$ and c is number of input channels) consists of a padded convolutional layer (kernel size = k_P) that doubles the number of channels. This is succeeded by batch normalization and application of Leaky ReLU activation. This is then followed by strided convolution (kernel size = k_S) for learnt-downsampling before being fed to an Inception-Residual Block to produce the block’s output feature map $f_{C_{n+1}^{c'}}$, where $c' = 2c$.
- 3) **Expanding Convolutional Block (ECB):** Each Expanding Convolutional Block (E_n^c) has a padded convolution layer of kernel size k_P that halves the number of channels, followed by batch normalization and leaky ReLU activation. Strided transposed convolution of kernel size k_{S^T} further reduces the number of channels by half after which the Inception-Residual Block follows. Each input feature map to the Expanding Convolutional Block consists of $f_{E_{n-1}^c} + f_{C_n^c}$, where $m = N - (n - 1)$. This represents concatenation of the output feature map of the previous ECB with the output feature map of the corresponding CCB in the contracting path. This allows for projection of features learnt at different stages of the contracting path onto the final feature map. The

¹All convolutions refer to one dimensional convolutions unless specified.

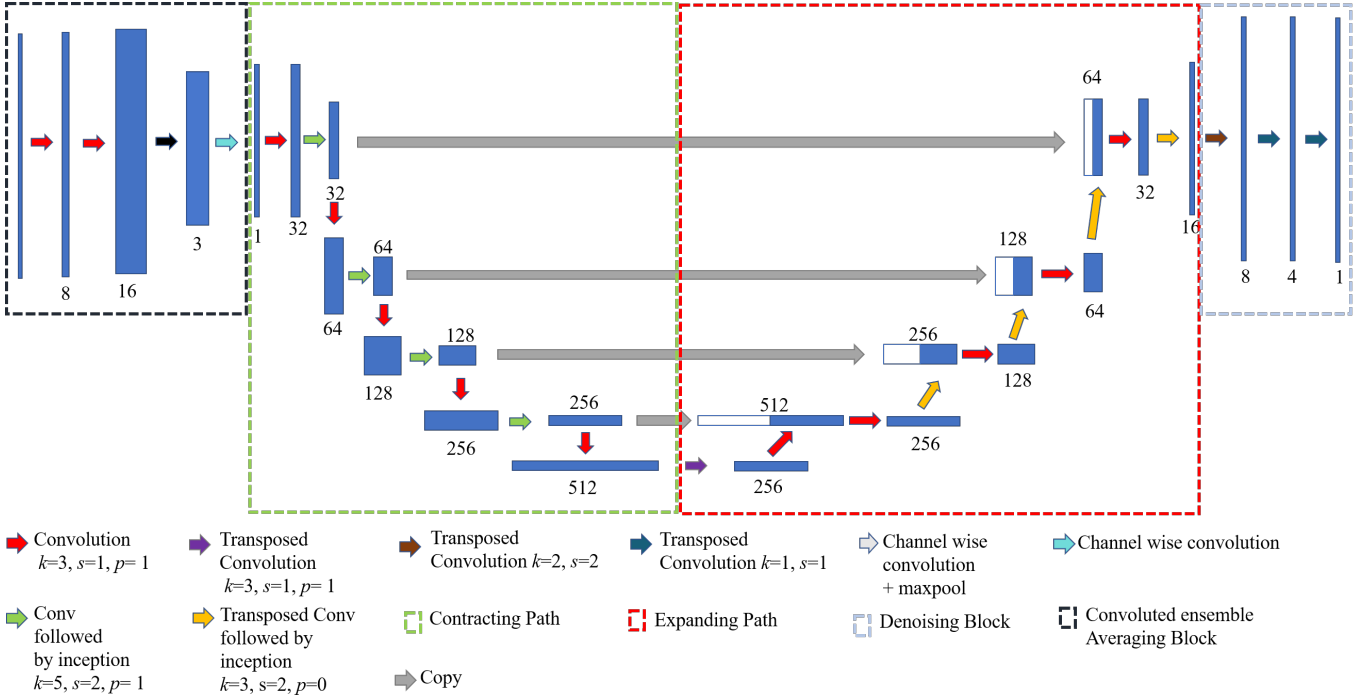


Fig. 3. SeismoNet Architecture (k -kernel size, s -stride, p -padding)

output feature map of this block is given by $f_{E_n^{c'}}$, where $c' = c/4$

- 4) **Convolutional Ensemble Averaging Block:** This block prepares the input signal to be fed to the contracting path. Ensemble Averaging is a statistical method used to improve the Signal to Noise Ratio by averaging out multiple versions of the same signal [28]. Retaining this intuition, the number of channels of the input signal is increased by passing it through a convolutional layer. Following this, convolution across the channels is performed which yields a surrogate signal that is jitter free with more prominent peaks, allowing for faster convergence during training.

- 5) **Denoising Block:** This block serves two purposes.
- 1) It allows for a better representation of the output from the U-net, ultimately producing a less distorted signal.
 - 2) It allows for learnt-upsampling, since the output of the U-net does not match the dimensions of the input signal exactly.

The input signal of length w is fed to the Convolutional Ensemble Averaging Block, which generates a feature map to be passed onto the first CCB in the contracting path. The feature map is passed through multiple CCBs until $n_{CCB} = N$, in which case the contracting path terminates and the expanding path begins. The input to the first ECB in the expanding path is the output feature map of the final CCB in the contracting path f_N^M , where $M = 2^{N-1} \times c_i$ and c_i is the number of output channels of the first CCB. Similar to the contracting path, the feature map is passed through multiple ECBs until

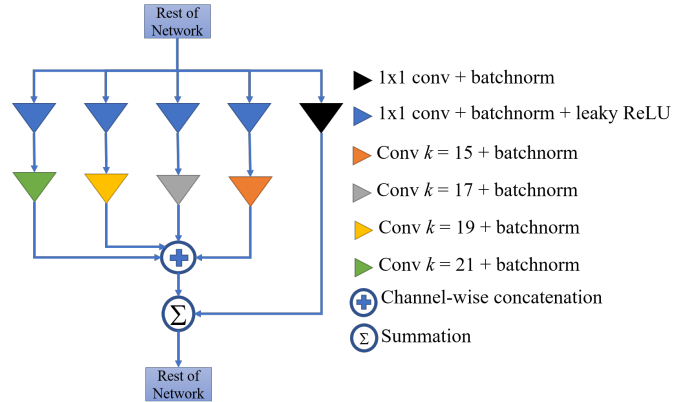


Fig. 4. Inception Residual Block

$n_{ECB} = N$. The final output signal is generated by passing the output of the final ECB to the denoising block. The final output signal has the same dimensions as the input signal.

V. EXPERIMENTS AND RESULTS

A. Implementation

For our experiments, $N = 5$ was chosen which results in a total of 12 blocks. Within each CCB and ECB, we select k_P to be 3 and both k_S and k_{ST} to be 5. The number of output channels of the first CCB (c_i) is chosen to be 32. The weights of the model were initialized in accordance with the Xavier uniform initializer [29]. Stochastic Gradient Descent with an initial learning rate of 0.001 was used to

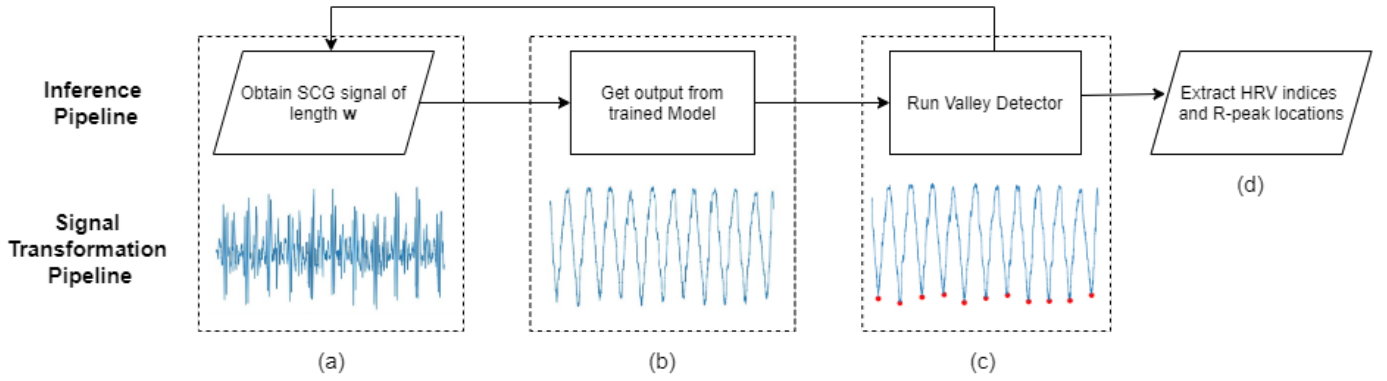


Fig. 5. Inference Pipeline

optimize the weights of the model by minimizing the loss given by Equation 1. SeismoNet was trained for 300 epochs with a learning rate scheduler which reduced the learning rate by a factor of 10 after every 100 epochs. These constants were empirically decided after extensive experimentation.

B. Inference

As stated in section IV-B the output waveform of the model yields information pertaining to the ECG signal. To obtain the output waveform, an SCG signal of window length w (Fig. 5a) is extracted and passed through SeismoNet. SeismoNet generates an output waveform of the same length w as shown in Fig. 5b. The valleys of the output waveform are detected to identify the R-peaks. The following subsections evaluate the different aspects of the model's performance.

C. R-peak Detection

1) *Metrics*: Sensitivity (Se) and Positive Predictive Value (PPV) were used to assess the model's efficacy in making accurate R-peak predictions whilst maintaining an immunity to falsely detected and missed peaks. If SeismoNet's detection falls within 90 ms [13] of the actual peak, it is classified as a True Positive (TP), otherwise it is classified as a False Positive (FP). Actual peaks which have been omitted from the predictions are classified as False Negatives (FN). Sensitivity and Positive Predictive Value are used to quantify SeismoNet's R-peak detection performance. The Sensitivity and Positive Predictive Value are defined using equations (3) and (4) respectively.

$$Se = \frac{TP}{TP + FN} \quad (3)$$

$$PPV = \frac{TP}{TP + FP} \quad (4)$$

2) *Performance*: Table I shows the performance of the model on the Test Set across all users. The total number of R-peaks in the test set was 6438 out of which 6323 were correctly detected. The sensitivity ranges from 0.94 in the case of subject 1, all the way to 0.99 for multiple subjects. Similarly, the lowest PPV was observed to be 0.95 for Subject

TABLE I
R-PEAK DETECTION PERFORMANCE ACROSS ALL USERS

Subject	Total Detected Peaks	Total Actual Peaks	TP	FP	FN	Se	PPV
1	319	323	304	15	19	0.94	0.95
2	317	316	309	8	7	0.98	0.97
3	367	368	365	2	3	0.99	0.99
5	373	375	370	3	5	0.99	0.99
6	323	323	318	5	5	0.98	0.98
7	269	270	267	2	3	0.99	0.99
8	515	516	510	5	6	0.99	0.99
9	321	321	318	3	3	0.99	0.99
10	311	310	306	5	4	0.99	0.98
11	368	368	361	7	7	0.98	0.98
12	443	440	432	11	8	0.98	0.98
13	378	378	374	4	4	0.99	0.99
14	351	350	344	7	6	0.98	0.98
15	337	337	334	3	3	0.99	0.99
16	390	391	387	3	4	0.99	0.99
17	356	353	345	11	8	0.98	0.97
19	348	344	336	12	8	0.98	0.97
20	352	354	343	9	11	0.97	0.97
Total	6438	6437	6323	115	114	0.98	0.98

1 and ranged between 0.97-0.99 for all the other subjects. On further analysis of subject 1, it was observed that the SCG signal was corrupted with substantial noise. In spite of this, SeismoNet performed significantly better even in the presence of a strict tolerance of 90 ms.

D. HRV Indices Extraction

The most clinically significant HRV parameters in the time domain were extracted by analysing the R-peaks detected by the model. This was done in order to assess their serviceability, by comparing them with the actual HRV indices obtained from the ECG signal. The parameters considered are shown in Table II.

1) *HRV indices Performance*: To understand the agreement between the HRV indices extracted from the R-peaks gen-

TABLE II
HRV PARAMETERS

HRV Parameter	Definition
Mean NN (ms)	Arithmetic mean of all interbeat intervals
SDNN (ms)	Standard Deviation of all interbeat intervals
RMSSD (ms)	Root mean square of successive differences between heart beat intervals
pNN50	Ratio of total number of successive NN intervals whose difference exceeds 50 ms to the total number of NN intervals

TABLE III
HRV INDICES DERIVED FROM ECG AND SCG

HRV Indices	SCG		ECG	
	Mean	SD	Mean	SD
Mean NN (ms)	876.6189	108.5728	877.8914	108.6028
SDNN (ms)	67.2341	18.0767	50.5093	11.7741
RMSSD (ms)	77.3436	27.8062	41.0370	13.7633
pNN50	0.1720	0.0552	0.0925	0.0516

erated from the model (SCG-indices) and from the R-peaks annotated on the ECG (ECG-indices), a Bland-Altman analysis is carried out. In the Bland-Altman plot, the error between two corresponding quantities is plotted against their mean, which in turn is used to systematically identify outliers in the data. In our case, the two quantities were the subject-wise SCG-indices and ECG-indices. The Limits of Agreement (LoA) were chosen to be $\pm 1.96 SD$ which corresponds to a confidence interval of 95%. As seen from each plot in Fig. 6, the range of the LoA is sufficiently small indicating high agreement of the SCG-indices and ECG-indices. 100% of the points lie within the LoA in the plots corresponding to the mean NN and SDNN as seen in Figures 6a and 6b respectively. This implies a high correlation between the two quantities. From Fig. 6 it can also be seen that there is only one outlier in the plots of pNN50 and RMSSD. These points correspond to subject 1.

The absolute values of the SCG-indices and ECG-indices across all users are shown in Table III. The difference between the indices is negligible thus validating the performance of SeismoNet as a tool to obtain accurate HRV as well.

VI. CONCLUSION

A Deep Fully Convolutional Neural Network was designed for creating an end-to-end solution for continuously examining cardiac activity using SCG signals, in a manner that is convenient and robust. Our model, SeismoNet, was able to detect R-peaks from SCG signals from the CEBS dataset, with a total Sensitivity of 0.98 and Positive Predictive Value of 0.98. On further analysis using Bland Altman plots, it was found that the HRV parameters derived from the SCG signals and from the ECG signals showed high correlation, thereby validating their agreement and interchangeability. Therefore, SeismoNet facilitates continuous monitoring of cardiac motions with ex-

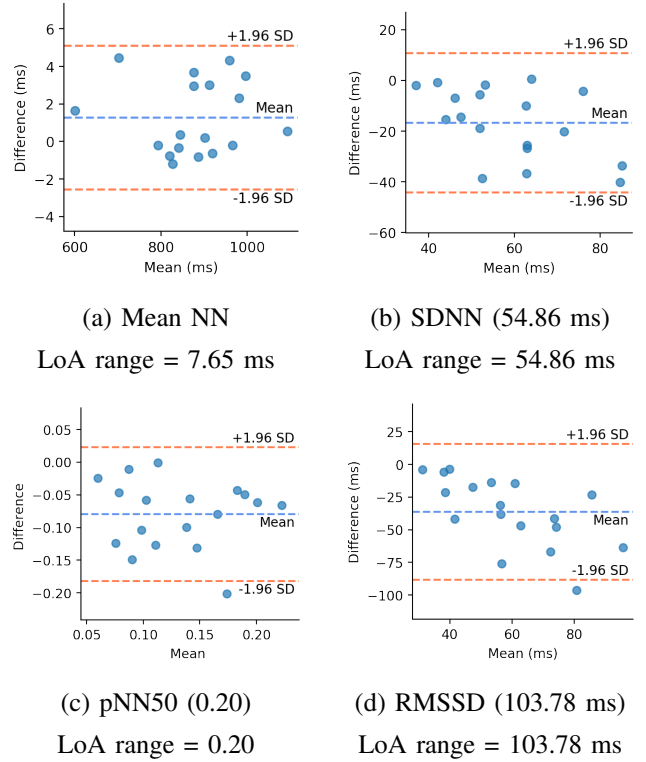


Fig. 6. Bland-Altman Plots of subject-wise HRV Indices with their corresponding range of LoA

ceptional accuracy while avoiding complex signal processing techniques and also keeping in mind the simplicity of such a system in real-world scenarios.

REFERENCES

- [1] V. Barauskienė, E. Rumbinaite, A. Karužas, J. Martinkutė, and A. Puodžiukynas, "Importance of heart rate variability in patients with atrial fibrillation," *Journal of cardiology & clinical research. San Diego: JSciMed Central*, 2016, vol. 4, no. 6, 2016.
- [2] G. Pal, P. Pal, N. Nanda, D. Amudharaj, and S. Karthik, "Spectral analysis of heart rate variability (hrv) may predict the future development of essential hypertension," *Medical hypotheses*, vol. 72, no. 2, pp. 183–185, 2009.
- [3] J. L. Mortara, "Ecg acquisition and signal processing," in *Cardiac Safety of Noncardiac Drugs*. Springer, 2005, pp. 131–145.
- [4] R. Sunkaria, S. Saxena, V. Kumar, and A. Singhal, "Wavelet based r-peak detection for heart rate variability studies," *Journal of medical engineering & technology*, vol. 34, pp. 108–115, 02 2010.
- [5] D. Widjaja, S. Vandeput, J. Taelman, M. A. Braeken, R. A. Otte, B. R. Van den Bergh, and S. Van Huffel, "Accurate r peak detection and advanced preprocessing of normal ecg for heart rate variability analysis," in *2010 Computing in Cardiology*, 2010, pp. 533–536.
- [6] C. H. Lund, L. B. Nonato, J. M. Kuller, L. S. Franck, C. Cullander, and D. K. Durand, "Disruption of barrier

- function in neonatal skin associated with adhesive removal,” *The Journal of pediatrics*, vol. 131, no. 3, pp. 367–372, 1997.
- [7] S. Sieciński and P. Kostka, “Determining heart rate beat-to-beat from smartphone seismocardiograms: Preliminary studies,” 10 2017, pp. 133–140.
- [8] Y. D’Mello, J. Skoric, S. Xu, P. J. Roche, M. Lortie, S. Gagnon, and D. V. Plant, “Real-time cardiac beat detection and heart rate monitoring from combined seismocardiography and gyrocardiography,” *Sensors*, vol. 19, no. 16, p. 3472, 2019.
- [9] M. J. Tadi, E. Lehtonen, T. Koivisto, M. Pänkäälä, A. Paasio, and M. Teräs, “Seismocardiography: Toward heart rate variability (hrv) estimation,” in *2015 IEEE International Symposium on Medical Measurements and Applications (MeMeA) Proceedings*. IEEE, 2015, pp. 261–266.
- [10] T. Koivisto, M. Pänkäälä, T. Hurnanen, T. Vasankari, T. Kiviniemi, A. Saraste, and J. Airaksinen, “Automatic detection of atrial fibrillation using mems accelerometer,” in *2015 Computing in Cardiology Conference (CinC)*. IEEE, 2015, pp. 829–832.
- [11] A. Q. Javaid, H. Ashouri, A. Dorier, M. Etemadi, J. A. Heller, S. Roy, and O. T. Inan, “Quantifying and reducing motion artifacts in wearable seismocardiogram measurements during walking to assess left ventricular health,” *IEEE Transactions on Biomedical Engineering*, vol. 64, no. 6, pp. 1277–1286, 2017.
- [12] M. J. Tadi, E. Lehtonen, T. Hurnanen, J. Koskinen, J. Eriksson, M. Pänkäälä, M. Teräs, and T. Koivisto, “A real-time approach for heart rate monitoring using a hilbert transform in seismocardiograms,” *Physiological measurement*, vol. 37, no. 11, p. 1885, 2016.
- [13] S. Siecinski, E. J. Tkacz, and P. S. Kostka, “Comparison of hrv indices obtained from ecg and scg signals from cabs database,” *BioMedical Engineering OnLine*, vol. 18, no. 1, p. 69, 2019.
- [14] M. Haescher, D. J. Matthies, J. Trimpop, and B. Urban, “A study on measuring heart-and respiration-rate via wrist-worn accelerometer-based seismocardiography (scg) in comparison to commonly applied technologies,” in *Proceedings of the 2nd international Workshop on Sensor-based Activity Recognition and Interaction*, 2015, pp. 1–6.
- [15] M. Haescher, D. J. Matthies, J. Trimpop, and B. Urban, “Seismotracker: Upgrade any smart wearable to enable a sensing of heart rate, respiration rate, and microvibrations,” in *Proceedings of the 2016 CHI Conference Extended Abstracts on Human Factors in Computing Systems*, 2016, pp. 2209–2216.
- [16] J. Hernandez, Y. Li, J. M. Rehg, and R. W. Picard, “Bioglass: Physiological parameter estimation using a head-mounted wearable device,” in *2014 4th International Conference on Wireless Mobile Communication and Healthcare-Transforming Healthcare Through Innovations in Mobile and Wireless Technologies (MOBI-HEALTH)*. IEEE, 2014, pp. 55–58.
- [17] J. Hernandez, D. J. McDuff, and R. W. Picard, “Biophone: Physiology monitoring from peripheral smart-phone motions,” in *2015 37th Annual International Conference of the IEEE Engineering in Medicine and Biology Society (EMBC)*. IEEE, 2015, pp. 7180–7183.
- [18] H. Lee, H. Lee, and M. Whang, “An enhanced method to estimate heart rate from seismocardiography via ensemble averaging of body movements at six degrees of freedom,” *Sensors*, vol. 18, no. 1, p. 238, Jan 2018. [Online]. Available: <http://dx.doi.org/10.3390/s18010238>
- [19] J. Yao, S. Tridandapani, W. F. Auffermann, C. A. Wick, and P. T. Bhatti, “An adaptive seismocardiography (scg)-ecg multimodal framework for cardiac gating using artificial neural networks,” *IEEE Journal of Translational Engineering in Health and Medicine*, vol. 6, pp. 1–11, 2018.
- [20] N. Mora, F. Cocconcelli, G. Matrella, and P. Ciampolini, “Detection and analysis of heartbeats in seismocardiogram signals,” *Sensors*, vol. 20, p. 1670, 03 2020.
- [21] M. Haescher, F. Höpfner, W. Chodan, D. Kraft, M. Aehnelt, and B. Urban, “Transforming seismocardiograms into electrocardiograms by applying convolutional autoencoders,” 04 2020.
- [22] J. Pan and W. J. Tompkins, “A real-time qrs detection algorithm,” *IEEE transactions on biomedical engineering*, no. 3, pp. 230–236, 1985.
- [23] F. Liu, C. Liu, X. Jiang, Z. Zhang, Y. Zhang, J. Li, and S. Wei, “Performance analysis of ten common qrs detectors on different ecg application cases,” *Journal of healthcare engineering*, vol. 2018, 2018.
- [24] M. A. García-González, A. Argelagós-Palau, M. Fernández-Chimeno, and J. Ramos-Castro, “A comparison of heartbeat detectors for the seismocardiogram,” in *Computing in Cardiology 2013*, 2013, pp. 461–464.
- [25] D. M. Gavrilă, “Multi-feature hierarchical template matching using distance transforms,” in *Proceedings. Fourteenth international conference on pattern recognition (Cat. No. 98EX170)*, vol. 1. IEEE, 1998, pp. 439–444.
- [26] P. F. Felzenszwalb and D. P. Huttenlocher, “Distance transforms of sampled functions,” *Theory of computing*, vol. 8, no. 1, pp. 415–428, 2012.
- [27] O. Ronneberger, P. Fischer, and T. Brox, “U-net: Convolutional networks for biomedical image segmentation,” in *International Conference on Medical image computing and computer-assisted intervention*. Springer, 2015, pp. 234–241.
- [28] T. Choudhary, M. K. Bhuyan, and L. N. Sharma, “Effect of respiratory effort levels on scg signals,” in *2019 IEEE Region 10 Symposium (TENSYP)*, 2019, pp. 143–146.
- [29] X. Glorot and Y. Bengio, “Understanding the difficulty of training deep feedforward neural networks,” in *Proceedings of the thirteenth international conference on artificial intelligence and statistics*, 2010, pp. 249–256.